MSE307 Engineering Alloys 2014-15 L8: Ti Alloy Mechanics II; Other Ti alloys

D. Dye[a]

[a]*Rm G03b, Department of Materials, Imperial College London, London SW7 2AZ, UK. david.dye@imperial.ac.uk*

In this last lecture we wrap up our discussion of the fatigue behaviour of titanium alloys by considering cold dell fatigue. Then, we consider defect modes in the production of titanium alloys, before turning away from $\alpha + \beta$ alloys to near-α, near-β and commercial purity (CP) titanium alloys.

8.1. Dwell Fatigue

Cold dwell fatigue is a failure mode that is occasionally of concern for titanium alloys, particularly those with high Al contents and small amounts of β phase. Primarily, in current usage, the issues are in Ti-811, IMI834 and in Ti-6242, which are all near-α alloys. It occurs at near-room temperature, when the material is subjected to sustained (several minute) holds in load at the peak stress during unnotched fatigue. The resultant drop in cyclic life can be around 10× or more, which is of great concern for compressor discs, because as we have seen, these are uncontainable if they fail in operation.

The high Al content of these alloys means that they can easily form α_2, and also that they lack β ligaments that might act as 'shock adsorbers' between the α grains. The dwell hold in load may be related to creep - at stresses near the yield stress α-Ti can shed applied loads quite quickly, as much as 150 MPa in a few minutes. Pace the Stroh model, we consider dwell fatigue to initiate when a grain that is soft-oriented forms a slip band, that then initiates faceting on the basel plane of an adjacent hard-oriented grain that is poorly oriented for slip.

Dwell fatigue is a poorly-understood phenomenon that is still the subject of research. In this lecture we will consider some aspects of the phenomenon, illustrated in some detail in a recent paper by Pilchak and Williams, published in 2011. They studied Ti-8Al-1Mo-1V bar that had been produced in a state that gave large numbers of macrozones, with alternating hard-oriented macrozones with their {0001} along the loading direction (bar axis) and those with their {0001} at 90° to the loading axis. This alloy possessed some secondary α in between $\sim 20\,\mu m$

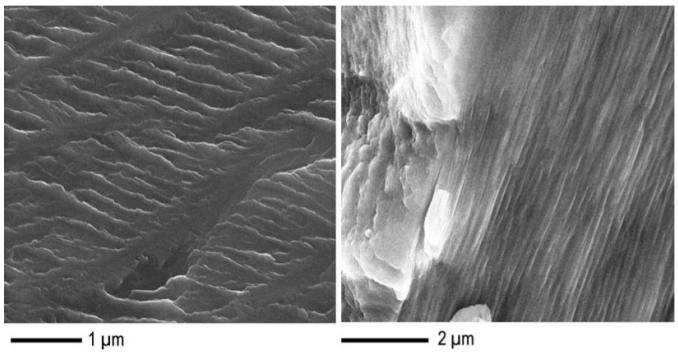

Figure 1: Striations formed in near-α Ti-8Al-1Mo-1V cycled in LCF at 95% of its static yield stress (758 MPa), R=0.1, 30 Hz. The sample fractured after 139,000 cycles. The striations spacing was $\sim 150\,nm\,cycle^{-1}$. From Pilchak and Williams, Metall. Mater. Trans A, 2011.

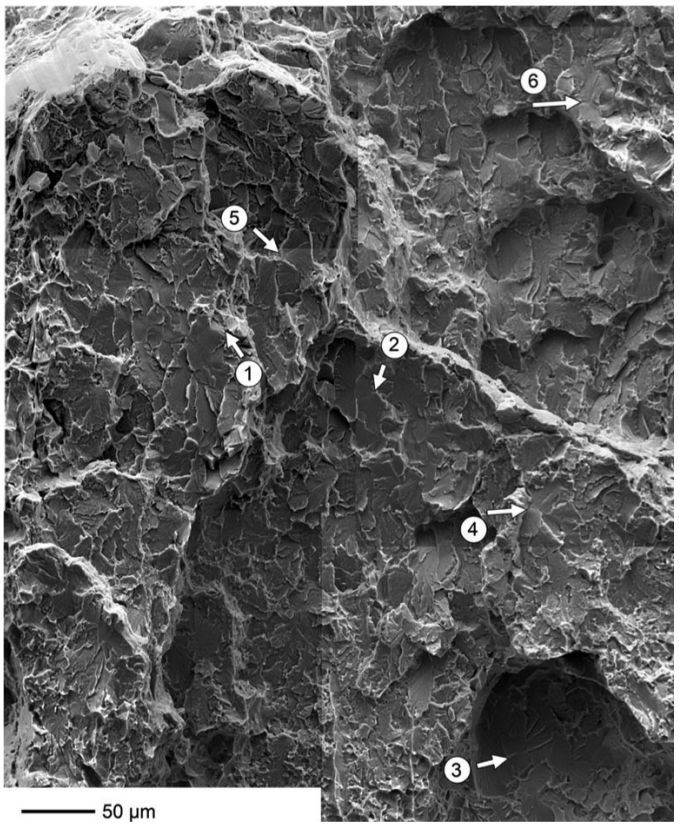

Figure 2: Near-α Ti-8Al-1Mo-1V cycled in LCF at 95% of its static yield stress (758 MPa), with 2 min dwells at peak stress, 1 s ramp-up, ramp-down and hold at the minimum stress (R=0.1). The sample fractured after 10,400 cycles, a dwell debit of 13×. The fracture surface was highly facetted, with a number of subsurface initiation facets (arrowed). From Pilchak and Williams, Metall. Mater. Trans A, 2011.

α_p grains, with thin β ligaments. They then tested it (i) in tension, (ii) on low cycle fatigue (LCF) and (iii) in dwell fatigue. Both the dwell and LCF tests used a load of 95% of the yield stress and $R = 0.1$, with the LCF tests at 30 Hz and the dwell tests have a 1-120-1-1 load cycle (1 s load-up, 120 s hold at load, 1 s unload and 1 s hold at the minimum stress). It was observed that the LCF sample endurance was 139,000 cycles, compared to only $10,400$ cycles in dwell, a debit of $13\times$.

Initially observing the fracture surfaces, the dwell facets tended to initiate subsurface, and multiple initiation was observed, with the cracks linking up as they grew. In comparison, LCF fracture sites were more nearly surface-initiating. The dwell fracture also 'tunnelled' along the hard-oriented macrozones, most likely because facetted fatigue crack growth is faster than striated fatigue crack growth. The LCF specimen growth facets showed evidence of striated crack growth, Figure 1, as in conventional fatigue.

The dwell primary initiation region is shown in Figure 2. Several secondary initiation sites (2-6) were observed; areas which cracked ahead of the growing crack tip but which were then overgrown by the dominant fatigue crack. The fracture generally has a more facetted appearance in dwell, as seen here. Now we turn to the initiating facet itself, Figure 3. The top figure shows the initiating facet for the LCF condition (top), and the tensile test piece (bottom). In both cases the initiation facet was near-{0001} and was relatively smooth. It neither case was the facet near-perpendicular to the loading axis, instead being inclined.

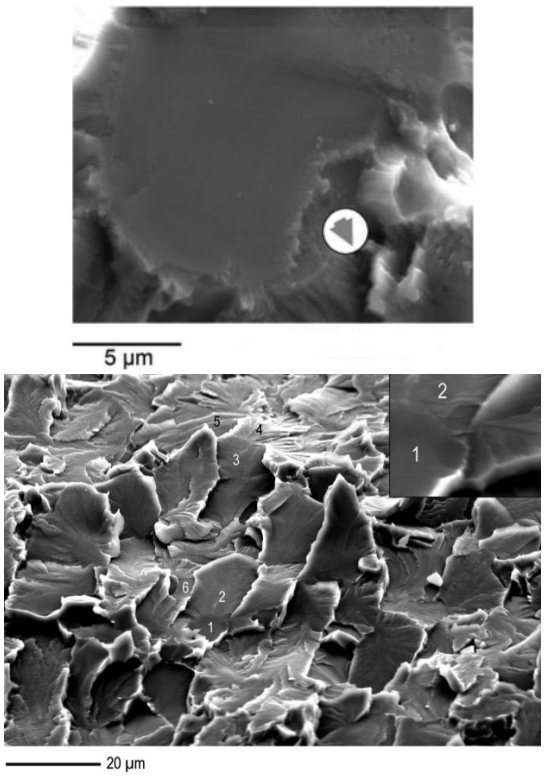

Figure 3: (top) Initiation facet in LCF specimen in Ti-811, and (bottom) the initiation region of the same material when tensile tested (inset showing the initiating facet). In both, the initiation facet was relatively featureless. From Pilchak and Williams, Metall. Mater. Trans A, 2011.

In Figure 4 a dwell initiating facet is examined (actually a secondary initiation site, but the primary initiation was similar, just harder to examine). B1 was the smooth initiation facet, whilst B2-B3 were growth facets with river lines. B1 is shown at a more favourable viewing angle at top right. The 'facet normal' inverse pole figure shows the crystallographic orientation of the facet normal (DW-B1, in red). The faceted grain crystallographic orientation in relation to the loading direction is also shown, 'loading direction IPF'. These show that DW-B1 was near-{0001}, and inclined 25° from the loading direction. It was also observed to be *extremely* smooth.

Therefore from this paper we can say that tensile, LCF and dwell facets are all near-{0001}, as were the HCF facets we saw in the last lecture. Here, the initiation facets in all three were inclined from the loading axis. In this paper, it is also suggested, quite convincingly, that H may be involved in the dwell fatigue process. H is held to enhance local plasticity near the crack tip, in common with stress corrosion cracking in chloride-containing environments, leading to easy slip localisation and therefore to easy facetting. There are hints that hydrides might form after cracking, condensing out of the material into the very high vacuum of a subsurface fatigue crack. The hydride habit plane is held to be 7-15° away from {0002}, and sometimes dwell facets seem to correlate with this plane. In any case, just like α_2 formation, the common thread to early failure modes in titanium are mechanisms that give rise to slip localisation, enhancing the basic lack of forest hardening of the α phase.

It is held by the aero-engine manufacturers that dwell fatigue can be observed in discs in spinning rig tests at very much lower stresses, and then that the {0001} facets are perpendicular to the loading axis, as suggested by the Stroh model. The fact that these were not observed in the present case is held to be due to the very high stresses used and the small volume of material tested. This presents a fundamental challenge to modern, small-scale low-cost university science, where ever-smaller testpieces are used and examined in ever-more detail by advanced in situ characterisation techniques such as X-ray diffraction - there we can only examine mechanisms, but not necessarily in the microstructural feature that actually gives rise to failure in real components.

8.2. Melt Anomalies

We have previously discussed one type of defect that can occurs in melting, hard α, when we discussed the Sioux City air accident. Another example of a melt-related defect is are high density inclusions (HDI). Classically, these are tungsten-rich inclusions arising from pieces of welding electrode (e.g. from the manufacture of the starting ingot)

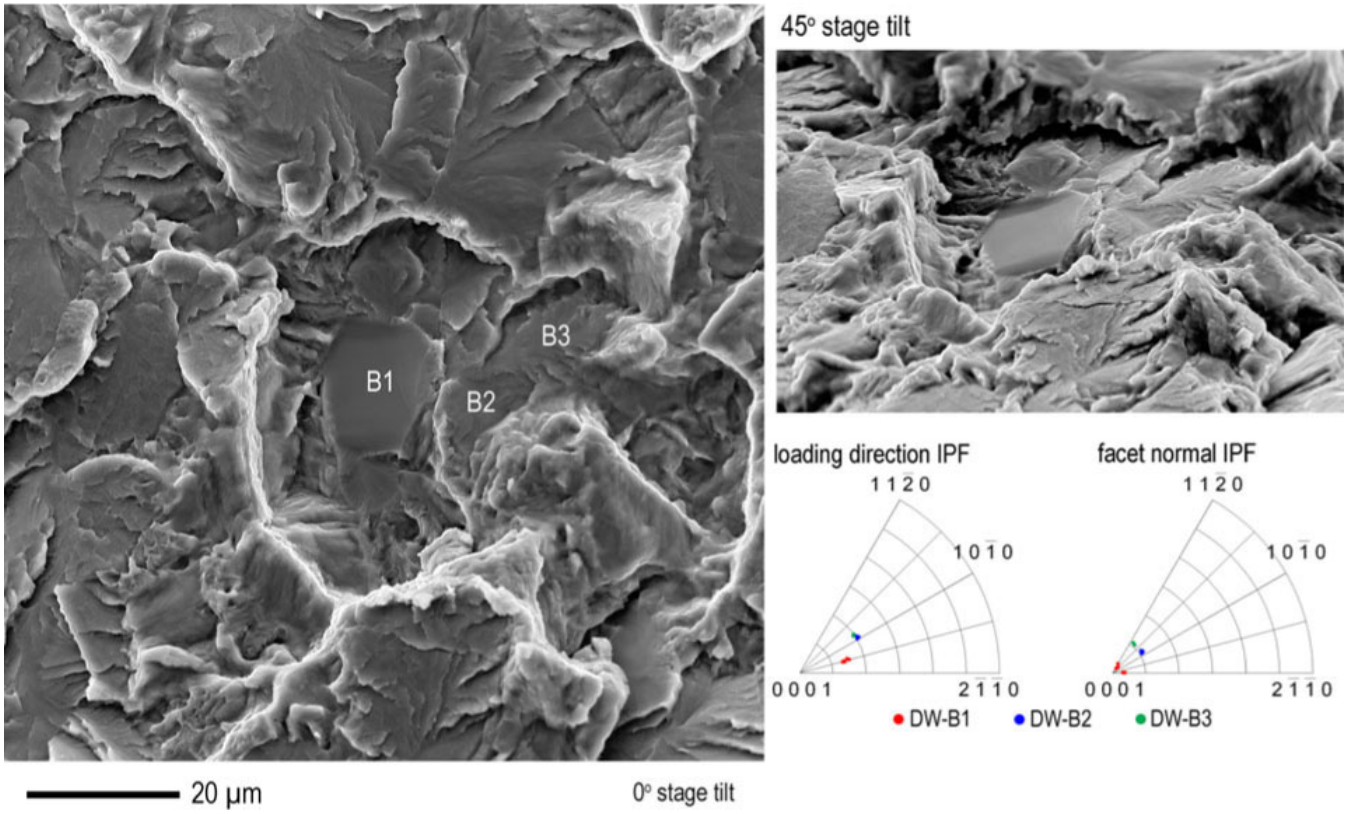

Figure 4: (Secondary) Initiation facet (DW-B1) in Ti-811 subjected to dwell fatigue. The facet was *very* featureless, was near-{0001} and inclined by 25° from the loading direction. From Pilchak and Williams, Metall. Mater. Trans A, 2011.

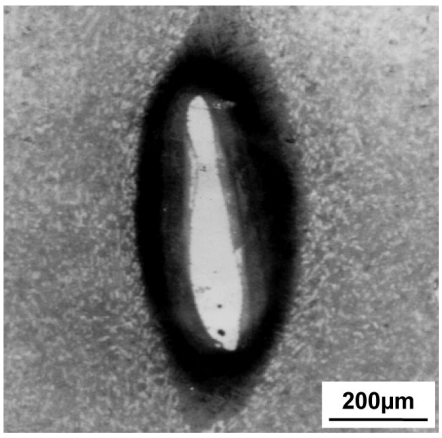

Figure 5: Example of a tungsten rich high density inclusion (HDI). Note that in this case, the inclusion has debonded from the surrounding matrix. From Lütjering and Williams.

or from WC tool bits incorporated into Ti turnings that are being recycled. Because of the high melting point of tungsten, the low superheat in VAR melts and the high density of tungsten, these can drop through the arc and molten pool to the bottom of the ingot with very little melt-back. An example is shown in Figure 5.

Due to the difference in thermal expansion between W and Ti, these HDI will often - but not always - debone from the surrounding Ti matrix, at which point the ingot will rattle! Often, they will end up at the bottom of the ingot, which is therefore discarded in some production schemes. Alternatively, in 'skull' melting processes like EBCHR they will drop into the cold Ti skull before he molten metal is poured. Otherwise, the historic approach is to ban 'revert' (the use of scrap) and to fanatically avoid the introduction of Ti into the manufacturing facility - e.g. in ball-point pens. Other, less extreme cases of HDI may occur with deliberate alloying additions such as Mo, if the starting materials used are too large to ensure melting during production.

Hard α, also called 'low density interstitial' defects are also melt-related and often relate to poor vacuum control in the Kroll sponge plant, water leaks, or to oxidation around welds due to poor welding practice during the fabrication of the initial ingot for VAR. Oxygen and nitrogen from this highly O/N-enriched particle - which is therefore brittle and entirely α phase - will then inter diffuse into the surrounding matrix. The hard α particle itself with then often crack and debone form the surrounding material, leaving a 100% α rim and a void, as in Figure 6. We have already discuss remediation measures when we discussed the Sioux City incident.

A third type of melt-related defect is beta fleck. The β eutectoid forming elements (Fe, Cr, Mn, Ni, Co) often also have a deep eutectic as well, resulting in an extended freezing range. This can result in very large levels of en-

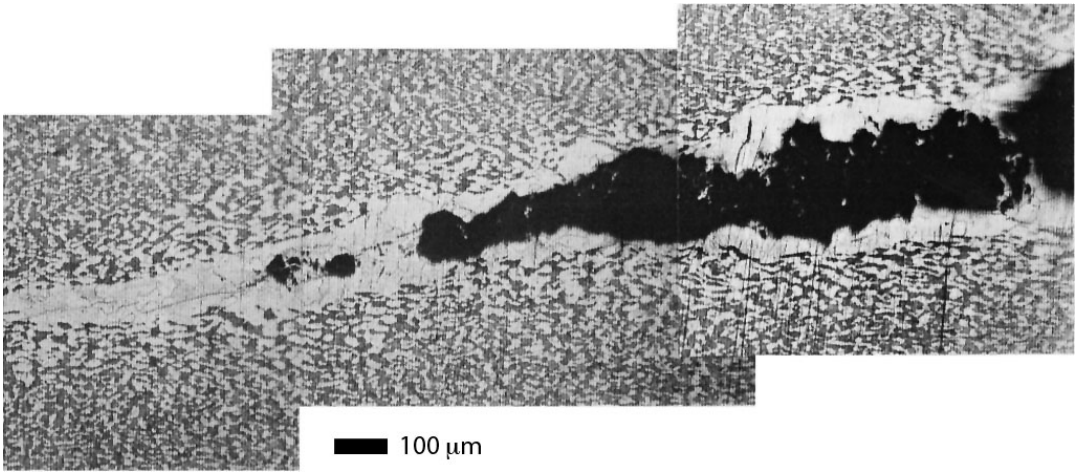

Figure 6: Example of a hard α inclusion, or LDI. In this case, the inclusion itself has been lost, leaving just the enriched α rim, which probably formed during high temperature deformation processing. Courtesy D Rugg.

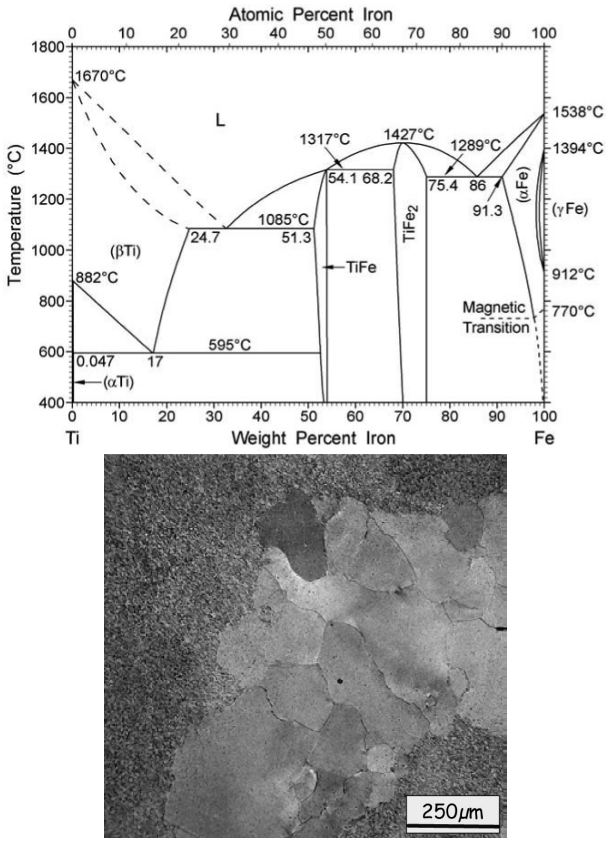

Figure 7: (top) The Ti-Fe phase diagram; note the deep eutectic, which is note observed for isomorphous stabilisers such as Mo. (bottom) example of a beta fleck defect in Ti-10V-2Fe-3Al, a type of segregation-related solidification defect. From Lütjering and Williams.

richment of the last liquid to solidify, and also long range macrosegregation in the ingot. There may also be a density effect, as with freckle defects in superalloys. In any case, the empirical observation is of 100% β regions, between several hundred micrometres to a few millimetres in size, that weaker and therefore lead to early crack initiation. An example, along with the Ti-Fe binary diagram (cf Ti-Mo), is shown in Figure 7. This is an example of a segregation defect, whose occurrence can be partly be controlled by control the solidification conditions (difficult in practice), but which mostly act to limit the freedom of the alloy designer.

As we complete our discussion of melt-related defects, it should be emphasised that the implication should not be taken that aviation safety is precarious or that flying is unsafe. The accident rate (accidents per million departures) declined from >30 in the early 1960s to <3 by the 1990s, and the decline continues today. Of course, it becomes ever-harder to eliminate the last, most uncommon and bizarre, possibilities in the fault tree, but continuous improvement and learning from incidents and accidents has made flying a very safe activity. Now, only 1 in 25 airframe hull losses have engine involvement. In 2013 (admittedly a good year), 224 people died in airline crashes - out of 3 billion on around 35 million flights. For comparison, over 400 people died in the US alone falling out of bed. And 2012 and 2011 were also very safe years. And when we have a bad patch - like the Malaysia airlines and Air Asia X accidents in 2014 - they often aren't mechanical in nature.

Sociologically, that isn't to say that the media attention paid to flying is unreasonable, or that the US reaction to 9/11 was necessarily wrong. Since Perrow's *Normal Accidents*, it's been recognised that we feel uncomfortable about risks taken on our behalf, where single incidents can result in large-scale loss of life, where there is associated dread ("radiation"), where the risks are novel (GM crops), or where the risks are borne by a different group to the beneficiaries (think cost-cutting by auto makers). Therefore many people are uneasy about nuclear power, nuclear weapons, aviation and corporate risk-taking out of all proportion to our attitude to, for example, road safety or dangerous sports. And so we continue to try to make

critical rotating parts in jet engines as reliably as possible, whilst continuing to improve their performance, so that we can make lighter, more fuel efficient jet engines.

8.3. CP Ti

Commercial purity (CP) Ti alloys are chiefly used for corrosion and static applications, such as in chemical plant, especially for salt water or chloride environments, and in cryogenic tanks in spacecraft. It accounts for the dominant non-aerospace use of titanium, typically in an α hot rolled and recrystallised condition such as that seen in Figure 8.

CP Ti grades are distinguished by their oxygen content, Table 1, and their tolerance for trace Fe left over from the parent rutile used in sponge production. As oxygen is a potent solution strengthener, and Fe helps reduce grain size, the strength rises significantly for the higher grades, but this come at a cost in ductility. The run-out HCF endurance is usually around 70% of the 0.2% proof stress. Often, people will quote oxygen contents in parts per million (ppm), by which they still mean by weight - so 1000 ppmw is the same as 0.1 wt.%. For O, the conversion from wt.% to at.% is about 3, so 2500 ppmw is about 0.75 at.% - this is worth remembering as this is about the limit beyond which interstitial solid solution strengthening by oxygen leads to strain localisation and severe loss of ductility.

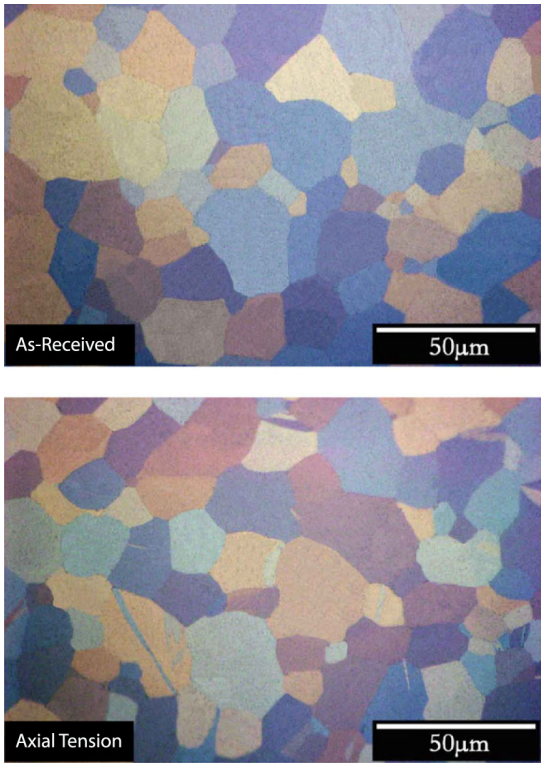

Figure 8: (top) Grade 1 CP Ti bar (Ti-0.04Fe-0.06O), in the as-recrystallised condition, (bottom) after deformation in tension, showing the appearance of twinning. From Wawrick et al, Dye research group, Acta Mater., 2012.

Grade	O (max) wt.%	Fe (max) wt.%	$\sigma_{0.2}$ MPa	UTS MPa	Elong. %	σ_{10^7} MPa
CP Ti Gr.1	0.18	0.2	170	240	24	-
CP Ti Gr.2	0.25	0.3	275	345	20	-
CP TI Gr.3	0.35	0.3	380	445	18	280
CP Ti Gr.4	0.4	0.5	480	550	15	350

Table 1: Compositions and mechanical properties of commercially pure titanium alloys. σ_{10^7} is the strength for an HCF life of $> 10^7$ cycles.

CP Ti alloys are also strengthened by grain size, as shown in Figure 9. For non-CP grades of 100% α alloys, substitutional strengthening with Al can be employed, but beyond an Al_{eq} of 5 wt.%, α_2 precipitates will be formed on ageing (or even slow cooling), which themselves do give precipitation strengthening but also, as discussed, lead to strain localisation and a loss of ductility. Finally, some strength optimisation can be obtained - in rolled CP Ti sheet the dominant texture places the {0002} near the ND, between the ND and TD. Unfortunately as this is the thin direction of sheet, this isn't often that useful in operation, but it can be very useful in sheet forming, as it means that CP Ti resists thinning quite effectively and is therefore quite formable.

This texture is quite different to Ti-6Al-4V, where the basal planes tend to lie in the transverse direction (a Basal / Transverse or B/T texture), and is common to that observed in zirconium alloys. This is the texture characteristic of the twinning modes in Ti - in fact, CP Ti undergoes c-axis deformation by twinning, mostly of the $\{10\bar{1}2\}$ and $\{11\bar{2}1\}$ types in tension and $\{11\bar{2}2\}$ in compression. Some twins can be observed in Figure 8. As the Al content is raised, or the O content, this acts to favour <c+a> slip over twinning.

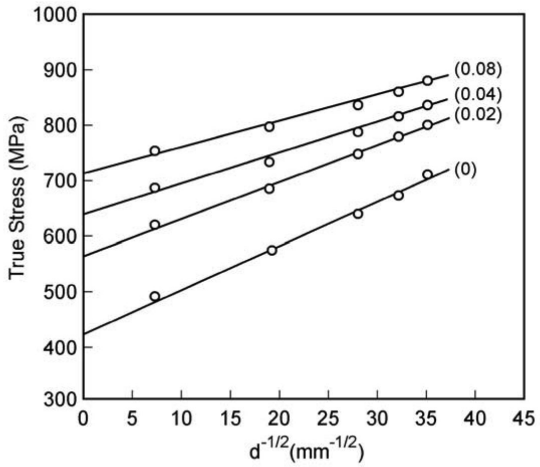

Figure 9: Hall-Petch relationship yield stress $\sigma_y = \sigma_0 + K/\sqrt{d}$ for CP Ti with different levels of plastic strain in CP Ti. From Lütjering and Williams.

8.4. Armour and High Rate Applications

Ti-6Al-4V was originally developed as an armour alloy for military applications where weight is critical, e.g. in armoured vehicles, and is widely used by the US military for this purpose. Here, aero-level defect control is not required and single melt material can be used, incorporating revert - which significantly reduces the cost (maybe as much as 10×?). Thinking about the performance of armour systems is actually quite complicated - at one extreme, dense, high kinetic energy projectiles may actually melt their way through a target. Back-side spall must be considered, just as in wooden battleships long ago. One response to this is to evaluate armour performance empirically - a common test is to evaluate the thickness of material required to defeat a threat projectile at a given velocity 50% of the time (this velocity is then termed v_{50}.

For example, against 14.5 mm armour piercing rounds at $v_{50} = 3200$ fps (975 m s^{-1} or 1670 mph) would require only 51 mm of Ti-6Al-4V of density 4.5, compared to 47.6 mm of RHA (rolled homogenous armour, AISI4340) steel plate of density 7.85, or 127 mm of aluminium (5883 series, density 2.7). This gives the Ti alloy a weight benefit of 60% over the steel (and Al only a 10% benefit). The exact performance increment varies depending on the threat, but typically increases for heavier threats, probably due to thickness effects.

The high strain behaviour of titanium alloys are also very important for fan blades in bird strike scenarios and for Ti casings in blade-off incidents.

8.5. Near-α Alloys

Near-α alloys are sometimes used in high temperature compressor applications. We will consider two alloys, IMI834 (Ti-5.8Al-4Sn-3.5Zr-0.5Mo-0.7Nb-0.35Si-0.06C, wt.%), and Ti-6242 (TI-6Al-2Sn-4Zr-2Mo-0.1Si), which are used at temperatures in the 400-600 °C range. They can be used in both a bimodal microstructure and in lamellar and equiaxed forms - examples are shown in Figure 10. The reason they are used is that they retain room temperature strengths of nearly 1 GPa, but with much better creep resistance than alloys containing the β phase - because self diffusion in the α is over 100× slower than in the β and so dislocation climb is much more difficult. Examine Figure 11, which is a Larsen-Miller plot of the lifetime at a given temperature and stress. Thus, for a 1000 h life at 300 MPa, Ti-6Al-4V would have a temperature capability of under 400°C whilst IMI834 would achieve around 600°C.

Of course, these alloys are good α_2 formers (Figure 12) and so tend to be quite brittle, with poorer fatigue performance and a vulnerability to cold dwell fatigue - but they are intended for use in creep resisting high temperature applications, so this is tolerated. This Si content is intended to promote the precipitation of silicides in the β ligaments, reducing the occurrence of the grain boundary sliding and transgranular dislocation glide creep mechanisms.

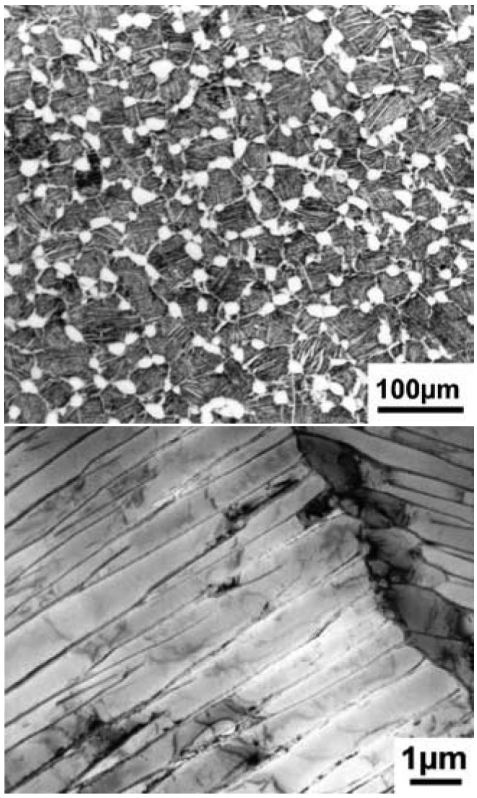

Figure 10: (top) IMI834 with a bimodal microstructure, and (bottom) Ti-6242 with a lamellar microstructure. Notice the very small β ligaments between the α plates. From Lütjering and Williams.

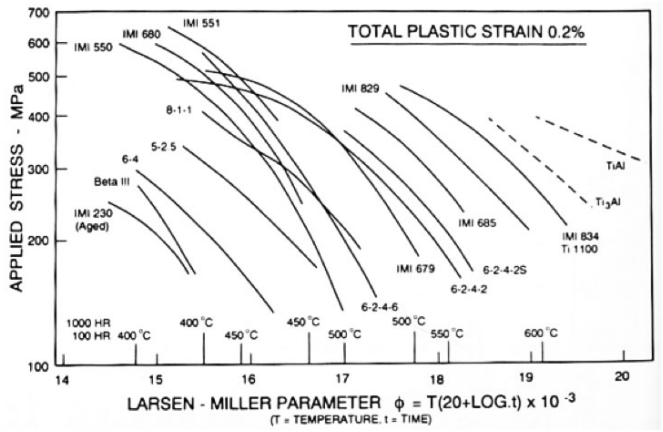

Figure 11: Larsen-Miller plot for titanium alloys, illustration the superior performance of near-α alloys like Ti-6242 and IMI834 over conventional $\alpha + \beta$ alloys like Ti-6Al-4V. From Flower.

8.6. Near-β landing gear alloys

The near-β alloys are heavily β-stabilised alloys that can often retain all all-β microstructure in optical microscopy on quenching. They are very strong, with yield strengths in excess of 1250 MPa and UTS of up to 1450 MPa, with $K_{1,c} \simeq 40\,\mathrm{MPa}\sqrt{\mathrm{m}}$. They are therefore becoming widely used for landing gear applications, replacing 300M (VAR AISI 4340) steel on specific strength grounds, and also because the anti-corrosion paints used are being banned

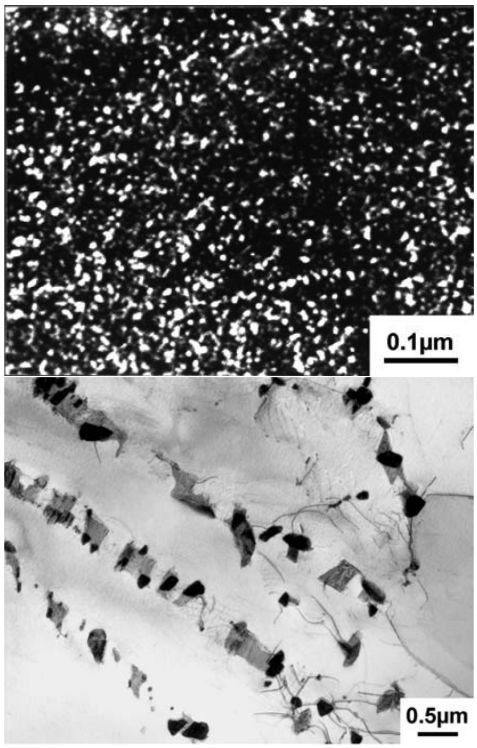

Figure 12: IMI834, TEM. (top) dark field image of α_2 after 24 h ageing at 700°C. (bottom) Bright field micrograph of $(TI,Zr)_5(Si_3$ precipitates that precipitated from the β ligaments at α plate boundaries after 2 h ageing at 700°C. From Lütjering and Williams.

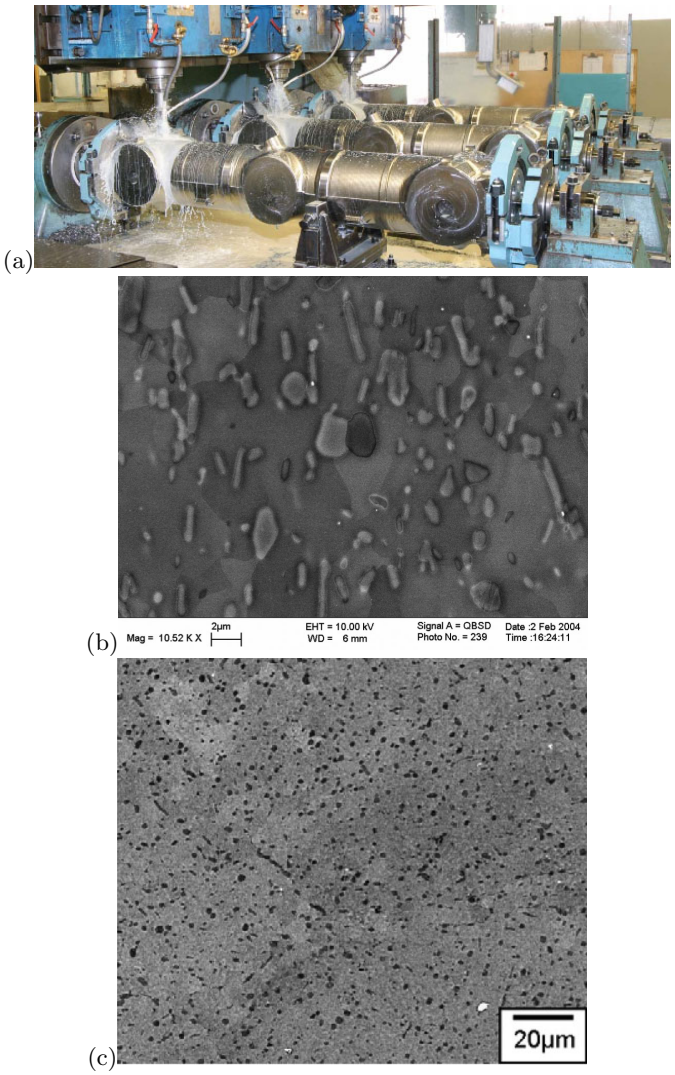

Figure 13: (a) Ti-5553 B787 8 ton truck beam forgings being machined. (b) Ti-10-2-3 as $\alpha+\beta$ forged, show β subgrains pinned by the globularised α_p, From Martin Jackson, Imperial College. (c) Ti-5553 as $\alpha+\beta$ forged (NG Jones, Dye research group, 2008).

due to the heavy metal content. As the landing gear account for 10% of total dry weight of the airplane, they are a significant item, with Ti-5553 truck beam forging now introduced on both the B787 and A350.

The alloys use α_p as nucleation agents for very fine secondary α that are developed on ageing; the α_p themselves do not contribute very much strength. Care must be taken in forging to avoid thick grain boundary α films. As the primary α plates are broken up and globularised during $\alpha+\beta$ forging, a β sub grain structure can be developed in Ti-10-2-3, Figure 13. Ageing then increases the strength from $\sim$ 850 MPa to $>$ 1250 MPa, as illustrated in Figure 14. The secondary α precipitated on the α_p are $<$ 50 nm across and therefore give very large amounts of Orowan strengthening ($\propto l^{-1}$).

A key feature of the high strength β alloys is that the kinetics are typically quite slow, allowing find control of the transformations to be achieved during low temperature ageing at 550-650°C. This is because of the addition of alloying elements like Mo in Ti-5Al-5Mo-5V-3Cr - an alloy such as Ti-10Fe-2Fe-3Al is regarded as harder to process because it lacks a slow diffuser like Mo.

8.7. Superelastic biomedical alloys

Finally, we turn to superelastic biomedical β-Ti alloys. This class of alloys are currently the topic of very much research, although they have yet to reach widespread application in patients. Two key exemplar alloys are Gum metal - Ti-36Nb-2Ta-3Zr-0.3O (wt.%) and Hao's Ti-2448 (Ti-24Nb-4Zr-8Sn, wt.%). These alloys are designed for low modulus, so as to minimise the stress shielding problem. Bone mass tends to decrease when it isn't loaded, and high-modulus implants will tend to unload the surrounding more compliant bone, resulting in osteolytic loosening of implants. The key insight is that as the outer $d-$electron per atom ratio e/a is decreased, then in β-Ti the C' modulus $(C_{11}-C_{12})/2$ decreases. Recall that C' is the $\{110\}[1\bar{1}0]$ shear modulus and is therefore also intimately bound up with the dislocation and ideal shear strength. Therefore heavily alloyed β Ti alloys can have moduli as low as 50-60 GPa, compared to 100-110 GPa for conventional titanium alloys. For example, the β phase in Ti-6Al-4V has the approximate composition Ti-20V and therefore has $C' \simeq 30$ GPa, Figure 15.

In fact, many of these alloys aren't particularly sta-

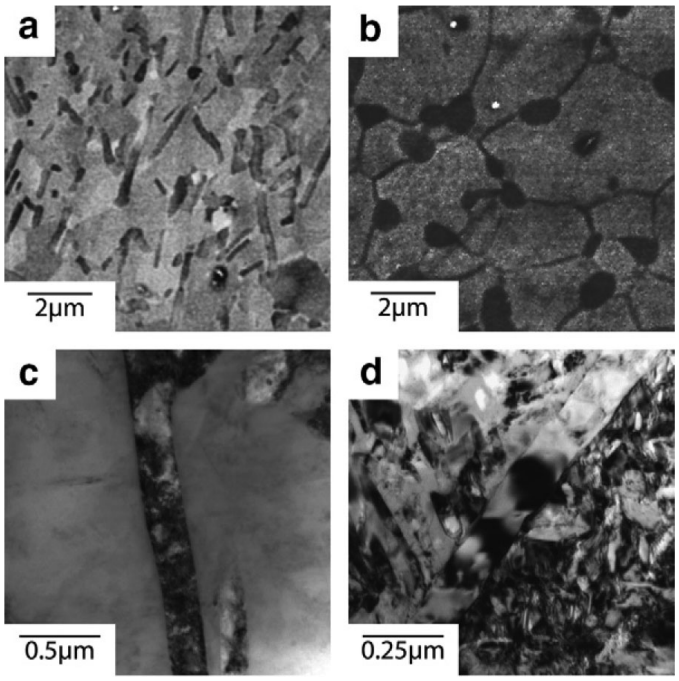

Figure 14: Microstructure of Ti-10-2-3 in the forged (left) and aged (right) conditions. Backscattered images from SEM (a-b) and TEM micrographs (c-d). From SL Raghunathan, Dye research group, 2007.

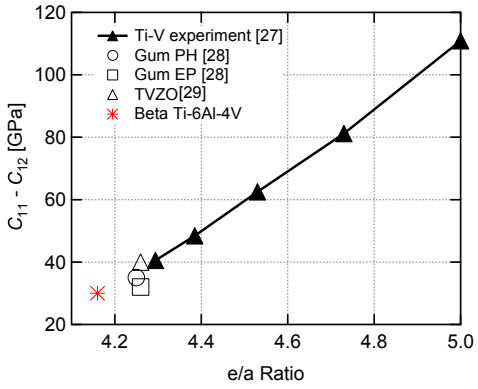

Figure 15: Effect of e/a ratio on C' in β-Ti. Pure Ti is at $e/a = 5$ whilst V (and other) alloying additions decrease e/a and the modulus C'. The Gum metal alloys are shown, as is the β phase in Ti-6Al-4V. The experimental data is from Collings. From Warwick et al, Dye research group, 2012.

ble. An interesting feature that was initially the subject of some controversy was that if they are examined carefully then that are actually found to be superelastic, that is, they undergo a reversible stress-induced phase transformation on loading, which gives rise to a kink in the stress-strain curve, Figure 16. On repeated loading the trigger stress decreases and it can be suppressed somewhat by O additions. The phase formed is an α'' orthorhombic martensite, depicted in Figure 20.

The stress-induced formation and disappearance of the α'' can be observed in situ using synchrotron X-ray diffraction, Figure 18. Some remnant α'' can be observed after

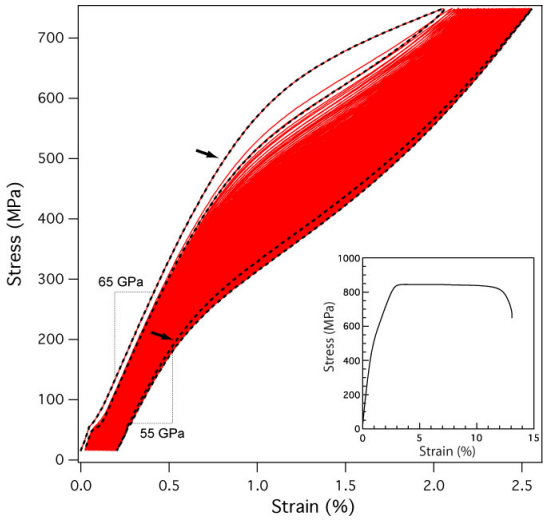

Figure 16: Gum metal in the as-extruded condition and cycled in LCF conditions for 200 cycles at 750 MPa (yield stress $\simeq$ 800-850 MPa. Note the deflection in the stress-strain surge, initially at around 500 MPa, the hysteresis on unloading and the drop in the trigger stress on repeated cycling. From VA Vorontsov et al, Dye research group, 2015.

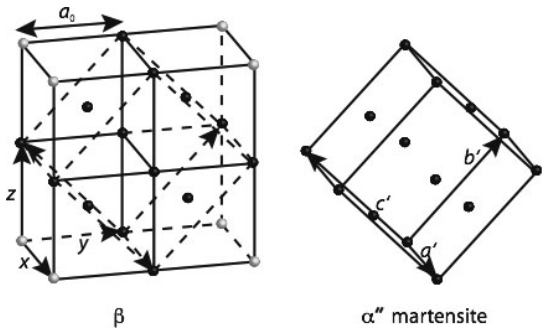

Figure 17: Prototype of the α'' orthorhombic martensite, showing the orientation relationship to the parent bcc β cell. From RJ Talling PhD thesis, Dye research group, 2012.

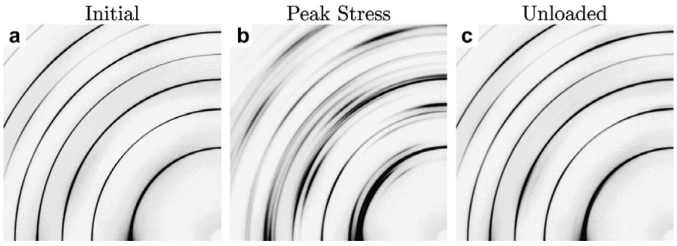

Figure 18: Appearance and disappearance of the α'' on loading and unloading in Ti-2448-0.08O; initially, only bcc rings appear in the diffraction pattern, at yield then additional rings due to the α'' are observed, which largely disappear on unloading. From Obbard et al, Acta Mater., 2011.

loading in TEM foils, Figure 19. The α'' are shown to form in self-accommodating twin-related laths, as in other martensites like NiTi and martensite in steels.

In general, as these alloys are vulnerable to shear, a whole group of shear-related phenomenon seem to co-occur.

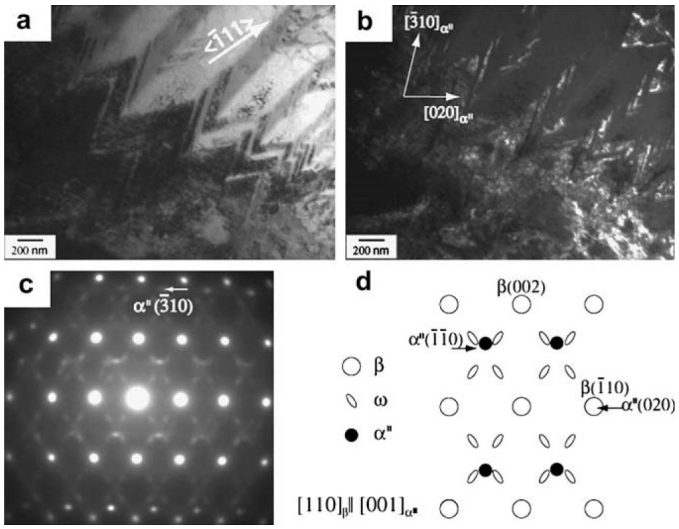

Figure 19: Loaded Gum metal showing the presence of α''. TEM bright field (a) and dark field (b) image obtained using the $(\bar{1}\bar{1}0)_{\alpha''}$ reflection. (c) the corresponding $[110]_{\beta}$ diffraction pattern and (d) key diagram, showing the location of the ω streaks and the α'' spots. From Talling et al, Dye research group, 2009.

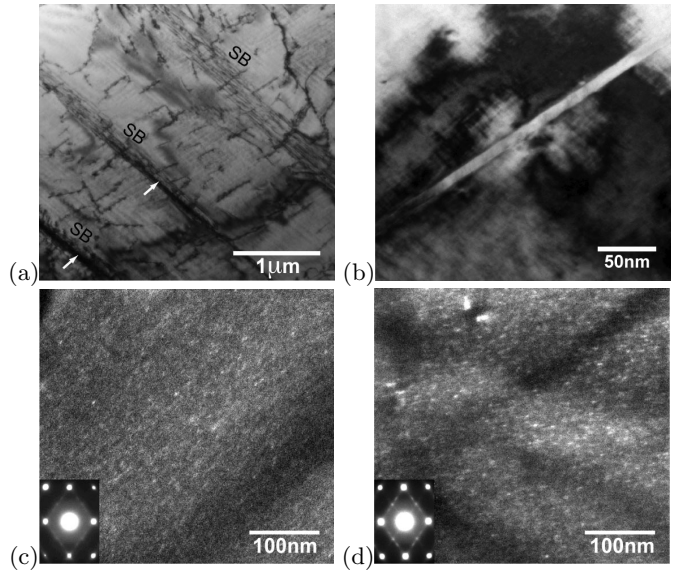

Figure 20: (a-b) Gum metal after 200 LCF cycles, (a) showing the presence of slip bands (SB) which were not present before deformation and (b) showing the presence of microtwins. (c) before loading, very faint ω streaking could be observed, which became much more prominent after cycling (d). From VA Vorontsov et al, Dye research group, 2015.

Slip bands and microtwins are also observed quite prominently, and by several authors. In addition, it seems that loading results in precipitation of the ω phase. Two explanations of this seem likely, either that the ω formation pressure has been lowered so far that ω can form in the stress field around dislocation cores or at α' interfaces; or that dislocation pipe diffusion has allowed isothermal ω formation to occur at an accelerated rate, or both.

It should be noted that in general these alloys lack the Al content that is supposed to suppress ω formation in the high strength β alloys; although in those we have shown that in the absence of α, ω can still be formed.

This class of alloys are fascinating and serve to illustrate the richness of the metallurgy that is accessible in the Ti alloy system.

8.8. Conclusions

We have concluded our examination of fatigue by considering dwell fatigue, after which we have engaged in a whistle-stop tour of non-$\alpha+\beta$ alloys - CP Ti, near-α, high strength β and the superelastic β alloys. This has brought us back to the consideration of defects that we began the lecture course with in Sioux City and in our consideration of melting and forging, and to consider fundamental alloys concepts like C' and e/a.

— END OF LECTURE —